ELSEVIER
J. Non-Newtonian Fluid Mech. xxx (2007) xxx–xxx
Journal of Non-Newtonian Fluid Mechanics
www.elsevier.com/locate/jnnfm

Nonlinear flow of wormlike micellar gels: Regular and chaotic time-dependence of stress, normal force and nematic ordering

Rajesh Ganapathy *, A.K. Sood

Department of Physics, Indian Institute of Science, Bangalore 560012, India

Received 30 October 2006; received in revised form 9 May 2007; accepted 19 May 2007

Abstract

We present our recent experiments on the nonlinear dynamics in the flow behaviour of shear-thinning wormlike micellar gels. In particular, we have shown experimentally that above a critical shear rate, the initial transient stress response comprises of overshoots and undershoots and this is followed by periodic, quasiperiodic, intermittent and chaotic behaviour. The normal force dynamics is similar to that of the stress. This can be classified as Type-II intermittency route to chaos. In our system, shear-thinning wormlike micellar solution of cetyltrimethylammonium tosylate, the strength of flow–concentration coupling is tuned by the addition of salt sodium chloride. The existence of a “butterfly” intensity pattern in small angle light scattering (SALS) performed simultaneously with the rheological measurements confirms the coupling of flow to concentration fluctuations in the system under study. Dynamic light scattering measurements to extract the relaxation time scales of concentration fluctuations are in excellent agreement with the in situ SALS measurements performed under shear. The scattered depolarised intensity in SALS, sensitive to orientational order fluctuations, shows the same time-dependence (like intermittency) as that of shear stress at various wave vectors.

Keywords: Rheochaos; Type-II intermittency; Stress relaxation; Wormlike micelles

1. Introduction

The rheological behaviour of wormlike micelles has aroused much attention in recent years. In response to large stresses, the flow behaviour of wormlike micelles is characterised by shear thinning or thickening, the presence of normal stress differences, flow-induced phase transitions and the phenomenon of shear banding. Systems of giant wormlike micelles formed in certain surfactant solutions are known to show very unusual nonlinear rheology. In measurements of the flow curve the stress is know to saturate beyond a critical shear rate, while the first normal stress difference increases roughly linearly with shear rate [1]. Cates and coworkers were the first to predict this kind of flow behaviour and they attribute this to a mechanical instability of the shear banding type [1]. In shear banding systems, the system splits into coexisting bands that support the same stress but have different average shear rates. The high shear rate band is lower in viscosity and shows a high degree of flow-induced alignment, while the low shear band has a higher viscosity and is the isotropic phase. Shear banding has been evidenced by flow birefringence [2] and nuclear magnetic resonance (NMR) velocimetry [3]. This kind of behaviour may be understood in terms of the reptation–reaction model which involves the reversible breakage and recombination of wormlike micelles along with reptation dynamics known for polymer solutions [4,5]. The flow curve can be measured under controlled stress or strain rate conditions. Depending on the time interval between the collection of data points, we can obtain metastable or steady state branches, respectively [6].

In shear-thinning wormlike micellar solutions of surfactant cetyltrimethylammonium tosylate (CTAT) that shows a plateau in the flow curve, Bandyopadhyay et al. found interesting time-dependence in the relaxation of the stress and normal force in step shear rate experiments for shear rate values fixed in the plateau region [7]. A time series analysis of the stress data using the time delay-embedding method, which can be easily done using the TISEAN software [8], showed the existence of a positive Lyapunov exponent, a measure of divergence of trajectories in phase space, and a fractal correlation dimension >2 implying that the signal was chaotic rather than the stochastic noise [9,10]. This has led to many theoretical [11–16] and experimental studies of this striking

* Corresponding author.
E-mail address: rajesh.ganapathy@gmail.com (R. Ganapathy).

0377-0257/$ – see front matter © 2007 Elsevier B.V. All rights reserved.
doi:10.1016/j.jnnfm.2007.05.008

Please cite this article in press as: R. Ganapathy, A.K. Sood, Nonlinear flow of wormlike micellar gels: Regular and chaotic time-dependence of stress, normal force and nematic ordering, J. Non-Newtonian Fluid Mech. (2007), doi:10.1016/j.jnnfm.2007.05.008

effect, termed *rheochaos,* in a wide variety of other systems including shear-thickening wormlike micellar solutions [17,18], lamellar, onion and sponge phases of surfactants [19–21] and dense colloidal suspensions [22]. NMR velocimetry and rheo-optical experiments suggest that rheochaos is closely linked to the phenomenon of shear banding [23–25] and have shown that the interface between the shear rate bands is not stable as predicted [1]. NMR velocimetry experiments, where the velocity profile across the gap is measured, have shown that the interface between the high shear rate band and the low shear rate band is spatio-temporally complex and this is accompanied by stress fluctuations [23]. This picture is also supported by the ultrasonic velocimetry experiments carried out by Bécu et al. [26] where the spatio-temporal dynamics of the high shear rate band was accompanied by stress fluctuations. Turbidity measurements on shear-thickening systems have yielded similar results [18,27]. Here, the turbidity of the sample is found to undergo time-dependent variations with the same period as the shear stress. Spatial heterogeneity should play a role in understanding rheochaos as exploited in recent theoretical models [11,13,15,28]. A recent experiment on wormlike micelles during flow start-up by Lerouge et al. [29] has shown that the interface amplitude is unstable and oscillates as a function of time, although they do not observe stress fluctuations.

Although rheochaos has been found in many experimental systems, the *route to rheochaos* has been found only recently [30]. These experiments have shown that the route to rheochaos in stress relaxation measurements is via time inverted Type-II intermittency for a shear-thinning wormlike micellar gel of surfactant CTAT in the presence of salt (NaCl). This system shows strong coupling of flow to concentration fluctuations evidenced by a “butterfly pattern” in small angle light scattering (SALS) measurements and a *power-law plateau* in the flow curve ($\sigma = \dot{\gamma}^{\alpha}$ where, σ is the stress and $\dot{\gamma}$ is the shear rate). The strength of the coupling can be tuned by the addition of salt sodium chloride (NaCl) [31]. In the present manuscript, we have carried out a more in-depth study of the SALS patterns reported earlier by performing dynamic light scattering measurements to extract the relaxation time scales of concentration fluctuations. These results are in excellent agreement with the in situ SALS measurements performed under shear [30]. We have also studied the initial transient stress response, comprising of overshoots and undershoots, for various step shear rates. Finally we also show qualitatively that the dynamics of the normal force is similar to the dynamics seen in the stress.

The intermittency route, of relevance here, is one of the three well-established routes to chaos. The intermittency route is characterised by turbulent bursts disrupting nearly periodic (laminar region) oscillations. Pomeau and Manneville [32] have established that within the intermittency route there are further three types. Type-I appears with an inverse tangent bifurcation, Type-II with a Hopf bifurcation and Type-III is associated with a period doubling bifurcation. Experimentally, all three types of intermittency have been observed in a variety of hydrodynamical and electrical systems [33–35].

2. Experimental

The sample preparation technique and the experimental procedures are described in detail in [30] and we will describe them only briefly here. The phase behaviour of CTAT has been well characterised [36]. CTAT forms cylindrical micelles that entangle to form viscoelastic gels for $c > c^* = 0.4$ wt.%. The CTAT/water and CTAT/NaCl/water samples were prepared by dissolving known amounts of CTAT (Sigma–Aldrich) in water and brine, and the viscoelastic gels formed were subsequently filtered to remove dust. The experiments were carried out on a MCR 300 stress-controlled rheometer (Anton PAAR, Germany) with small angle light scattering attachment (SALS) at a temperature of 26.5 °C. All experiments were carried out in a cylindrical Couette geometry with transparent top and bottom plates (inner cylinder diameter 32 mm, height 16.5 mm and gap 2 mm). A vertically polarised (V) laser beam ($\lambda = 658$ nm and spot size 1 mm) enters the gap between the cylinders (the beam is close to the inner rotating cylinder and cannot be translated across the gap) along the vorticity ($\nabla \times \mathbf{v}$) direction, where $\mathbf{v}$ is the velocity field. Polarised and depolarised light scattering studies are performed by analysing the scattered light in the ($\mathbf{v}$, $\nabla\mathbf{v}$) plane using a CCD camera. The images obtained are analysed in Matlab 6.1 (Mathworks Inc., USA) using home-written programs.

3. Results and discussion

The flow curves for pure CTAT 2 wt.% and CTAT 2 wt.% + 10 mM NaCl show a nearly flat stress plateau $\alpha = 0.05$ and 0.07, respectively [30,37]. The weak departure from a true plateau is due to the inhomogeneity of the stress field arising from geometry curvature [30,37,38]. Fig. 1a shows the flow curve for the CTAT 2 wt.% + 100 mM NaCl system. The stress shows a strong shear rate dependence ($\alpha = 0.32$ for CTAT 2 wt.% + 100 mM NaCl) above $\dot{\gamma} > 1\ \mathrm{s}^{-1}$ which cannot be attributed to geometry effects [38]. We attribute this slope to a concentration difference between the bands [38–40] arising from a Helfand–Fredrickson mechanism [41–43] (see [30] for a detailed discussion). This is also borne out by our SALS experiments which show a “butterfly” light scattering pattern with the wings of the butterfly stretched along the flow direction [44]. Fig. 1b shows the evolution of the SALS intensity pattern in the VV geometry along the flow curve for the CTAT 2 wt.% + 100 mM NaCl sample. In the Newtonian regime of the flow curve the scattered intensity pattern is symmetric as expected (Fig. 1b1, the small notch is an artifact due to a reflection of the laser beam from the inner wall). At the plateau onset, $\dot{\gamma} = 2\ \mathrm{s}^{-1}$, the SALS pattern is elongated along the flow direction implying coupling of flow to concentration fluctuations (Fig. 1b2). At $\dot{\gamma} = 10\ \mathrm{s}^{-1}$, we see a clear “butterfly” light scattering pattern and two bright regions about the center and along the flow (Fig. 1b3).

Fig. 2 shows the intensity distribution along the flow direction for the “butterfly” pattern shown in the inset. The bright lobe corresponds to the peak in the intensity pattern. The origin behind the peak is the following: for flow–concentration coupling, the stress relaxation time τ_{stress} should be less than the time scale due to concentration fluctuations $\tau_{\mathrm{conc}} = 1/Dq^2$,

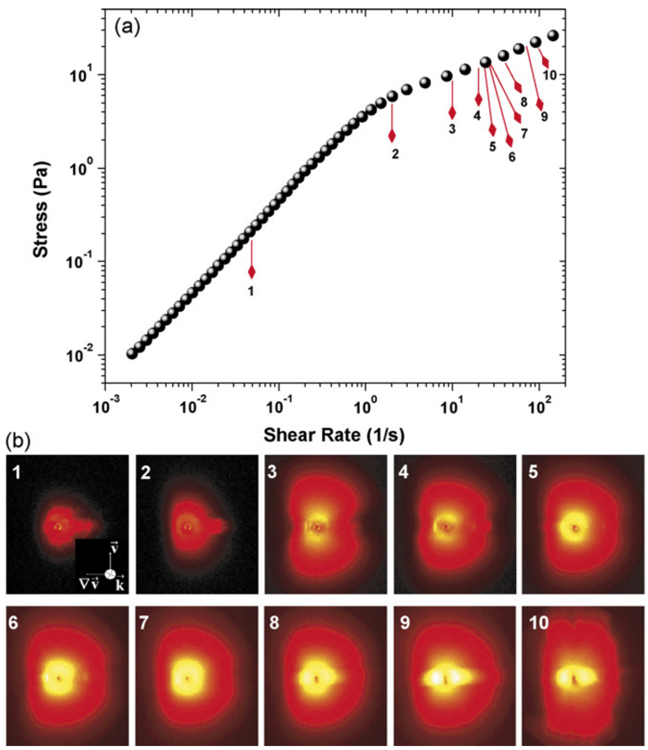

Fig. 1. (a) Flow curve for CTAT 2 wt.% + 100 mM NaCl. (b) Evolution of SALS profiles for CTAT 2 wt.% + 100 mM NaCl. (1) 0.05 s^{-1}, (2) 2 s^{-1}, (3) 10 s^{-1}, (4) 20 s^{-1}, (5) 23 s^{-1}, (6) 25 s^{-1}, (7) 27.5 s^{-1}, (8) 40 s^{-1}, (9) 70 s^{-1}, and (10) 100 s^{-1}.

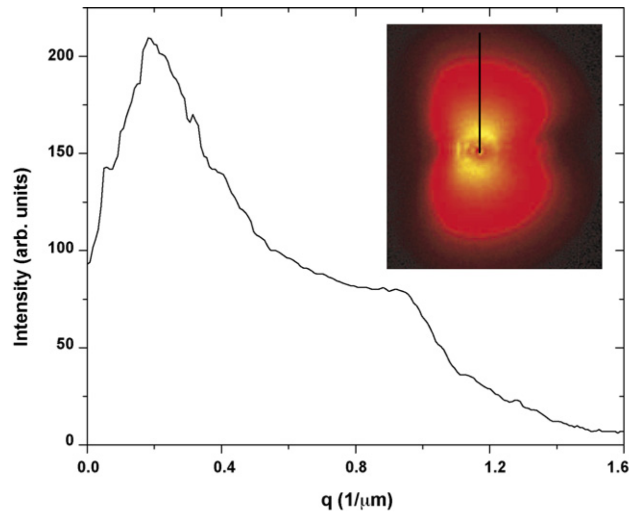

Fig. 2. Structure factor $S(q)$ for the CTAT 2 wt.% + 100 mM sample at $\dot{\gamma} = 10\,s^{-1}$. (Inset) "Butterfly" pattern. The intensity was calculated along the flow (denoted by black line).

where D is the diffusion coefficient. This is always valid at small wave vectors. At large wave vectors, concentration fluctuations decay faster than stress and the flow–concentration mechanism fails and the scattered light intensity decreases. The peak thus corresponds to a wave vector q^* at which $\tau_{stress} = \tau_{conc} = l/Dq^{*2}$. The diffusion coefficient D due to concentration fluctuations can be estimated from the decay of the fastest mode in dynamic light scattering (DLS) experiments and the stress relaxation time τ_{stress} can be obtained from a linear rheology experiment. Fig. 3a and b shows the intensity autocorrelation function from DLS and the frequency response from linear rheology for the CTAT 2 wt.% + 100 mM NaCl sample, respectively. The diffusion coefficient obtained by fitting a single exponential to the initial decay is $D = 1.67 \times 10^{-11}\,m^2/s$. The peak in the structure factor, corresponding to $\tau_{stress} = \tau_{conc}$, of Fig. 2 is at a wave vector $q^* = 0.2\,\mu m^{-1}$ and thus $\tau_{conc} = l/Dq^{*2} = 1.42$ s. This is in excellent agreement with the stress relaxation time $\tau_{stress} = 1$ s determined from linear rheology (Fig. 3b). Returning to Fig. 1, the bright lobes in the SALS pattern at higher shear rates (Fig. 1b4–8)are symmetric and this could be due to the contribution from orientational fluctuations [45]. At the highest shear rates, although the overall SALS profile is stretched along the flow, the bright region at the center is extended in a direction perpendicular to flow and this could be due to the formation of a shear-induced 1D gel phase [46]. We have carried out experiments at six different salt concentrations 10 mM < c_{NaCl} < 1 M, which yield plateau slopes ranging from $0.07 < \alpha < 0.4$. We find that a minimum slope of 0.12, corresponding to a salt concentration of 25 mM NaCl, is essential to see a "butterfly" pattern indicating the onset of flow–concentration coupling at this α value.

To ensure that the slope of the plateau is not a transient, we have carried out controlled-shear rate flow experiments on the CTAT 2 wt.% + 50 mM NaCl sample at different waiting times per point. To measure a steady-state flow curve in an experiment, the stress/shear rate has to be swept extremely slowly. Typically the waiting time per data point should be many times the Maxwell time [6]. For systems that show flow–concentration

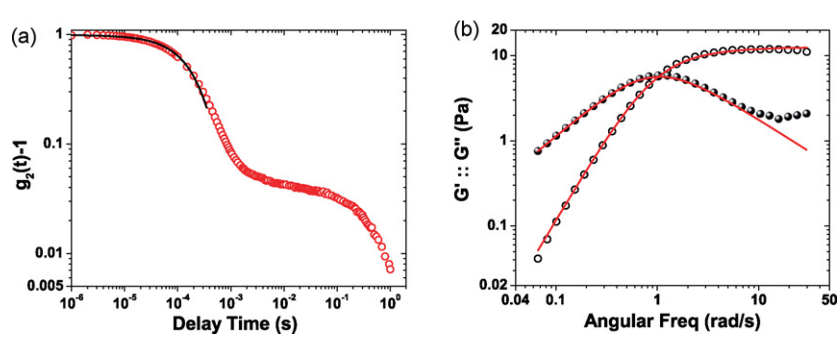

Fig. 3. (a) Intensity autocorrelation function at $\theta = 60°$ (black line exponential fit) and (b) frequency response measurement (lines denote Maxwell fits) for CTAT 2 wt.% + 100 mM NaCl sample.

Please cite this article in press as: R. Ganapathy, A.K. Sood, Nonlinear flow of wormlike micellar gels: Regular and chaotic time-dependence of stress, normal force and nematic ordering, J. Non-Newtonian Fluid Mech. (2007), doi:10.1016/j.jnnfm.2007.05.008

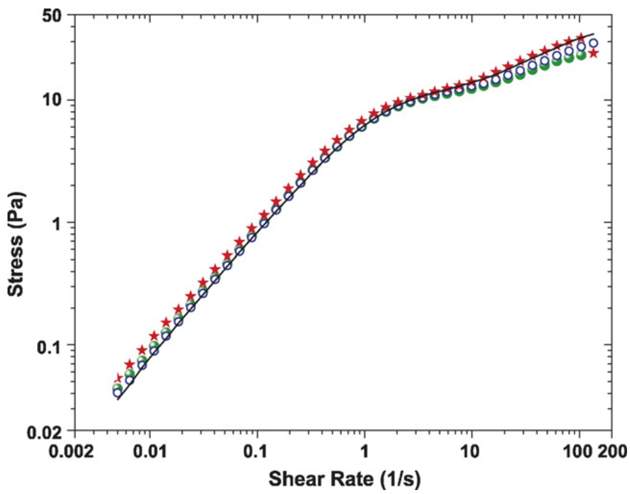

Fig. 4. Shear rate controlled flow curves at different waiting times. $\Delta t = 30$ s (solid circles), $\Delta t = 60$ s (hollow circles), $\Delta t = 120$ s (stars) and $\Delta t = 180$ s (line).

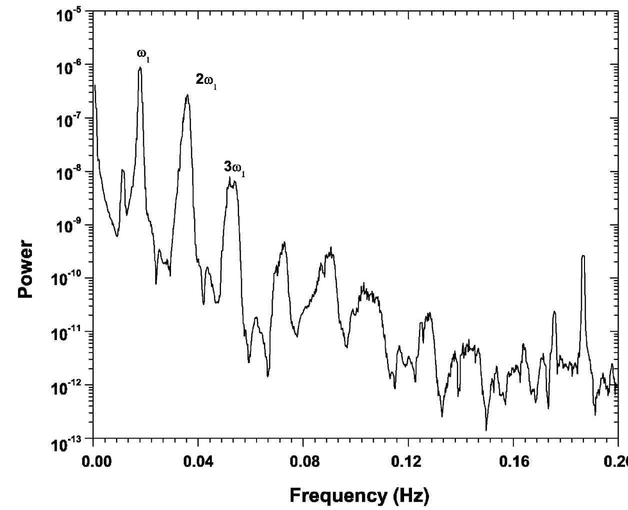

Fig. 6. Fourier power spectrum of data shown in Fig. 5e.

coupling the waiting time should be long enough to attain diffusive equilibrium across the whole shear cell. Fig. 4 shows the flow curves carried out at four waiting times. All the flow curves overlap in the Newtonian regime. The plateau slope increases marginally ($\alpha = 0.21$ for $\Delta t = 30$ s and $\alpha = 0.29$ for $\Delta t = 180$ s) as the waiting time is increased and we also see deviations in the high shear region of the flow curve. For waiting time $\Delta t > 120$ s, the flow curves overlap over the complete range of shear rates studied, implying an approach towards steady-state behaviour.

Now we turn to our results from stress relaxation experiments. Fig. 5 shows the stress relaxation dynamics for the CTAT 2 wt.% + 50 mM NaCl sample at different shear rates. This sample shows a stress plateau in the flow curve with $\alpha = 0.24$, implying flow–concentration coupling. The stress time series remains flat in the Newtonian region (Fig. 5a). Just at the plateau onset and beyond, the stress shows oscillations with a very large time period that reduces with increase in shear rate (Fig. 5b and c). At a shear rate of $\dot{\gamma} = 10\,\mathrm{s}^{-1}$ (Fig. 5e), the stress oscillations look nearly periodic and this is seen in the corresponding Fourier power spectrum (Fig. 6). With increase in shear rate, the stress signal shows dynamics suggesting quasiperiodicity. Fig. 7 shows the power spectrum of the signal shown in Fig. 5f. We see that there are two primary frequencies centered around $\omega_1 = 0.030$ Hz and $\omega_2 = 0.033$ Hz and their higher harmonics. Fig. 8 shows a similar power spectrum with two frequencies centered around $\omega_1 = 0.036$ Hz and $\omega_2 = 0.041$ Hz at a $\dot{\gamma} = 17\,\mathrm{s}^{-1}$

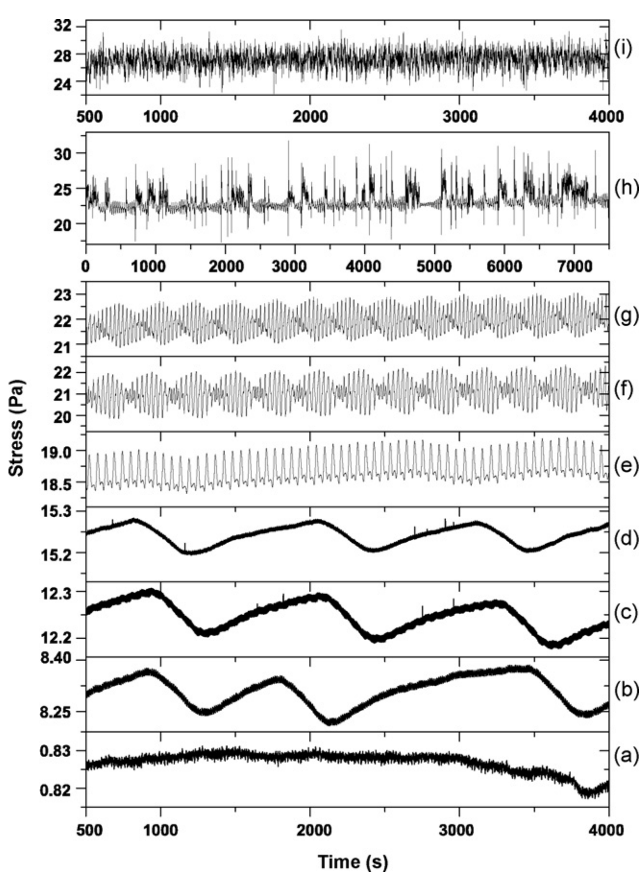

Fig. 5. Stress relaxation at various shear rates for CTAT 2 wt.% + 50 mM NaCl. (a) $\dot{\gamma} = 0.05\,\mathrm{s}^{-1}$, (b) $\dot{\gamma} = 0.75\,\mathrm{s}^{-1}$, (c) $\dot{\gamma} = 2\,\mathrm{s}^{-1}$, (d) $\dot{\gamma} = 5\,\mathrm{s}^{-1}$, (e) $\dot{\gamma} = 10\,\mathrm{s}^{-1}$, (f) $\dot{\gamma} = 15\,\mathrm{s}^{-1}$, (g) $\dot{\gamma} = 17\,\mathrm{s}^{-1}$, (h) $\dot{\gamma} = 19\,\mathrm{s}^{-1}$, and (i) $\dot{\gamma} = 21\,\mathrm{s}^{-1}$.

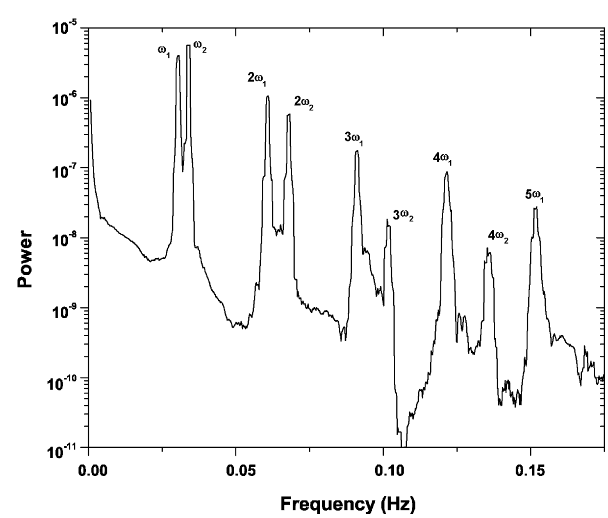

Fig. 7. Fourier power spectrum of data shown in Fig. 5f.

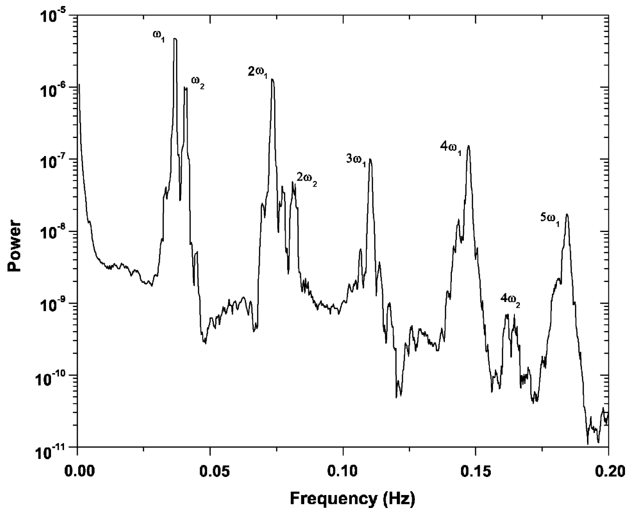

Fig. 8. Fourier power spectrum of data shown in Fig. 5g.

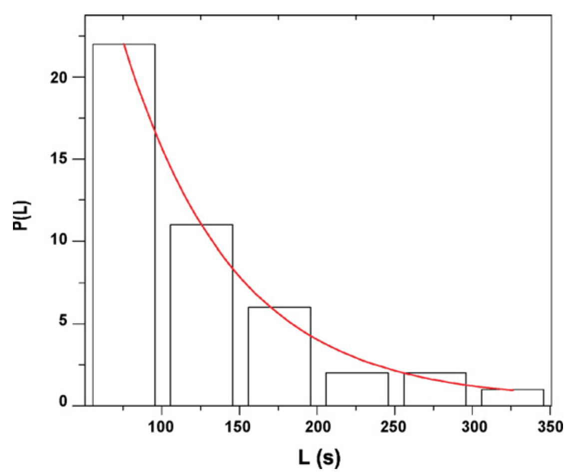

Fig. 9. Probability distribution of laminar lengths L of data shown in Fig. 5h. The red line is the exponential fit. Figure adapted from Ref. [30].

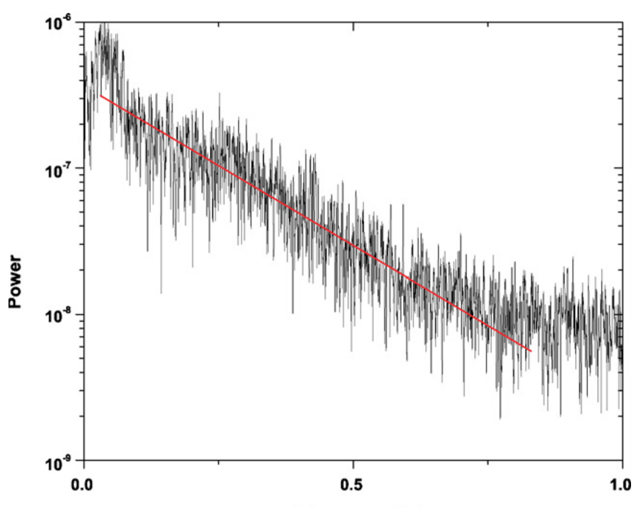

Fig. 10. Fourier power spectrum of data shown in Fig. 5i.

(Fig. 5g). We would like to mention here that in all our step shear rate experiments, the "butterfly" pattern is seen throughout the course of the run and is not a transient phenomenon that occurs during flow start-up or stop [44]. This might be due to the fact that the shear band themselves are spatio-temporally non-stationary. In Fig. 5h we show the time series obtained at $\dot{\gamma} = 19\,\mathrm{s}^{-1}$ in a 2 h run. There are ≈50 bursts of chaos disrupting nearly periodic oscillations. This is characteristic of intermittency. Judging by the nature of the signal during the laminar phase, Type-III intermittency can be ruled out, since, for this type of intermittency there is a subharmonic mode with increasing amplitude. A standard test for analysing intermittent data is the probability distribution of laminar lengths L between burst events. The probability distribution of laminar lengths shows an exponential tail (Fig. 9) at large times. For Type-II intermittency the probability distribution of laminar lengths L scales as $P(L) \sim L^{-2}$ for small times and shows an exponential tail at larger times [47]. Also, Type-II intermittency is preceded by quasiperiodicity which has also been observed for the CTAT 2 wt.% + 50 mM NaCl sample. This strongly suggests that the sample is going through the Type-II intermittency route to chaos. At a higher shear rate, $\dot{\gamma} = 21\,\mathrm{s}^{-1}$ (Fig. 5i), the sample showed chaotic dynamics characterised by an exponentially decaying power spectrum (Fig. 10) [48].

In stress relaxation experiments on CTAT wormlike micellar gels, Bandyopadhyay et al. [7] found that the normal force

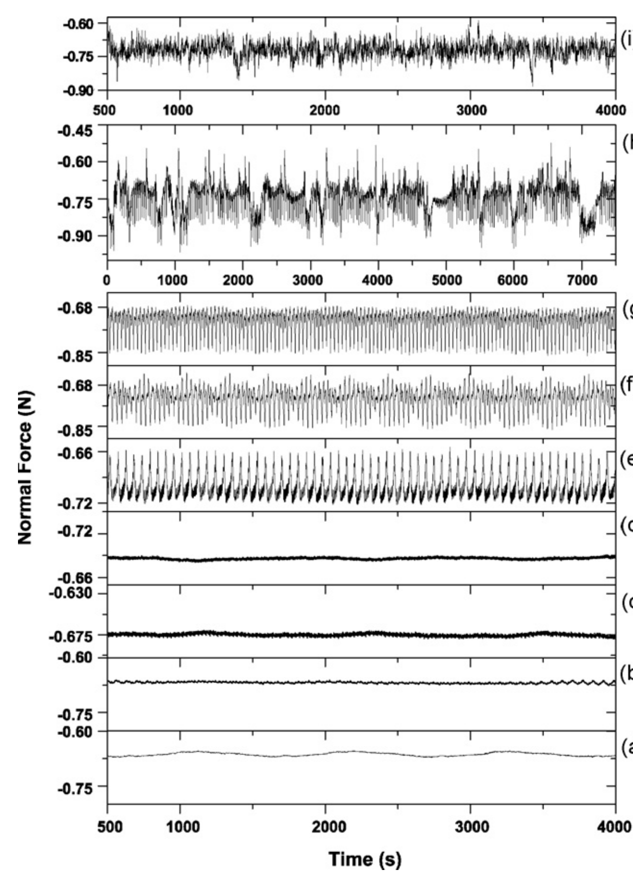

Fig. 11. Normal force at various shear rates for CTAT 2 wt.% + 50 mM NaCl. (a) $\dot{\gamma} = 0.05\,\mathrm{s}^{-1}$, (b) $\dot{\gamma} = 0.75\,\mathrm{s}^{-1}$, (c) $\dot{\gamma} = 2\,\mathrm{s}^{-1}$, (d) $\dot{\gamma} = 5\,\mathrm{s}^{-1}$, (e) $\dot{\gamma} = 10\,\mathrm{s}^{-1}$, (f) $\dot{\gamma} = 15\,\mathrm{s}^{-1}$, (g) $\dot{\gamma} = 17\,\mathrm{s}^{-1}$, (h) $\dot{\gamma} = 19\,\mathrm{s}^{-1}$, and (i) $\dot{\gamma} = 21\,\mathrm{s}^{-1}$.

Please cite this article in press as: R. Ganapathy, A.K. Sood, Nonlinear flow of wormlike micellar gels: Regular and chaotic time-dependence of stress, normal force and nematic ordering, J. Non-Newtonian Fluid Mech. (2007), doi:10.1016/j.jnnfm.2007.05.008

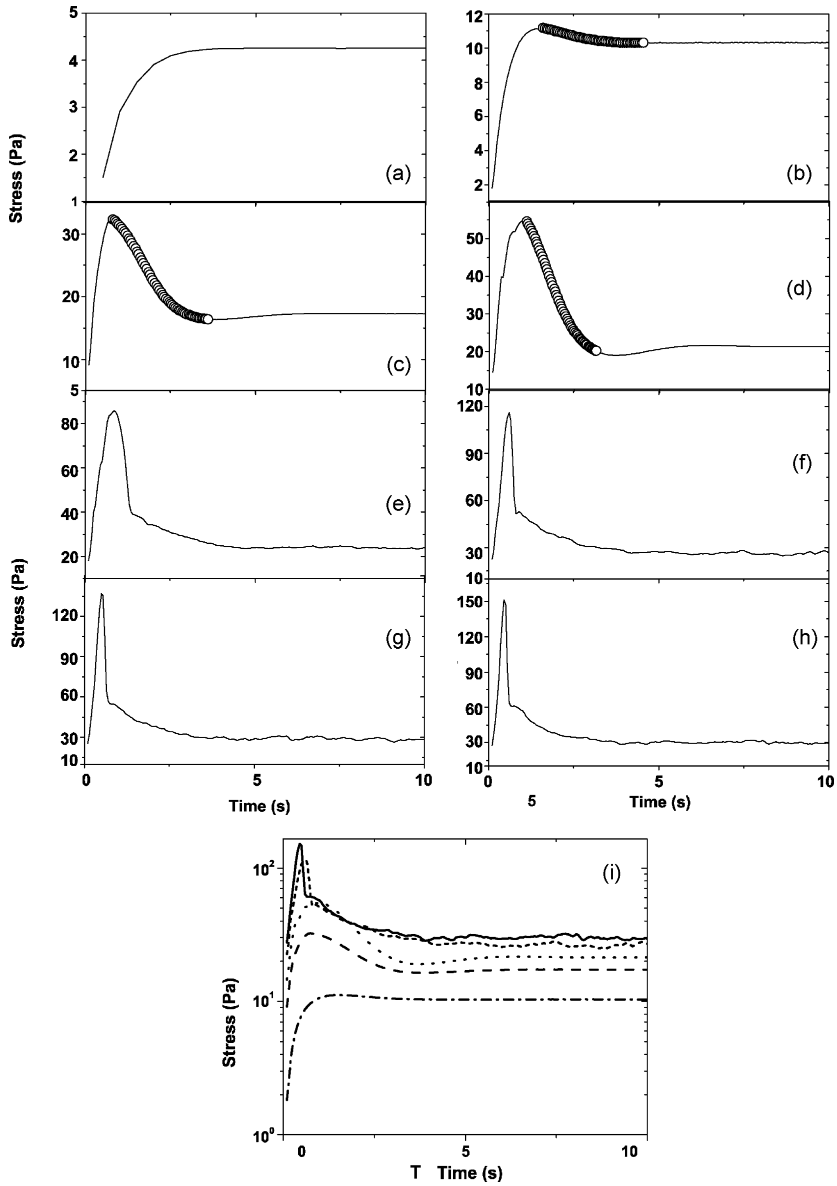

Fig. 12. Initial transient stress response on application of step shear rate for CTAT 2 wt.% + 100 mM NaCl system. (a) $\dot{\gamma} = 0.05\,\mathrm{s}^{-1}$, (b) $\dot{\gamma} = 2\,\mathrm{s}^{-1}$, (c) $\dot{\gamma} = 10\,\mathrm{s}^{-1}$, (d) $\dot{\gamma} = 16\,\mathrm{s}^{-1}$, (e) $\dot{\gamma} = 20\,\mathrm{s}^{-1}$, (f) $\dot{\gamma} = 25\,\mathrm{s}^{-1}$, (g) $\dot{\gamma} = 28\,\mathrm{s}^{-1}$, and (h) $\dot{\gamma} = 30\,\mathrm{s}^{-1}$. (i) Overlaid data of (b) (dash-dot), (c) (long dashes), (d) (dots), (e) (small dashes), and (f) (line). The sigmoidal fit (Eq. (1)) is shown by circles.

also displayed dynamics similar to the stress. Unlike their experiments which were done in a cone-plate geometry, our experiments have been performed in the cylindrical Couette geometry (recessed end) and hence the normal force cannot be measured very accurately. Nevertheless, the sample confined between the bottom plate and the bottom of the inner cylinder (a crude parallel plate arrangement, gap ≈ 1.5 mm) is large enough to yield a measurable normal force. We see that the normal force shows dynamics similar to that of the stress. Fig. 11 shows the normal force time series for the CTAT 2 wt.% + 50 mM NaCl sample at different shear rates. This normal force shows quasiperiodicity (Fig. 11f), intermittency (Fig. 11h) and chaos (Fig. 11i) analogous to shear stress, implying that elastic instabilities play a major role in rheochaos.

Before we delve into the stress relaxation dynamics at other salt concentrations, we would like to briefly discuss the initial transient response shown by the sample upon the application of a step shear rate. Fig. 12 shows the initial transient stress response before the stress settles down to a steady state value for the CTAT 2 wt.% + 100 mM NaCl sample. In the Newtonian region, $\dot{\gamma} = 0.05\,\mathrm{s}^{-1}$, the stress approaches the steady state monotonically (Fig. 12a). For stress values in the plateau region the stress shows an overshoot followed by a sigmoidal decay to the steady state. The sigmoidal fitting function is an S-shaped function and is given by

$$y = \frac{(A_1 - A_2)}{(1 + \mathrm{e}^{(x - x_0)/\tau_0})} + A2 \tag{1}$$

Please cite this article in press as: R. Ganapathy, A.K. Sood, Nonlinear flow of wormlike micellar gels: Regular and chaotic time-dependence of stress, normal force and nematic ordering, J. Non-Newtonian Fluid Mech. (2007), doi:10.1016/j.jnnfm.2007.05.008

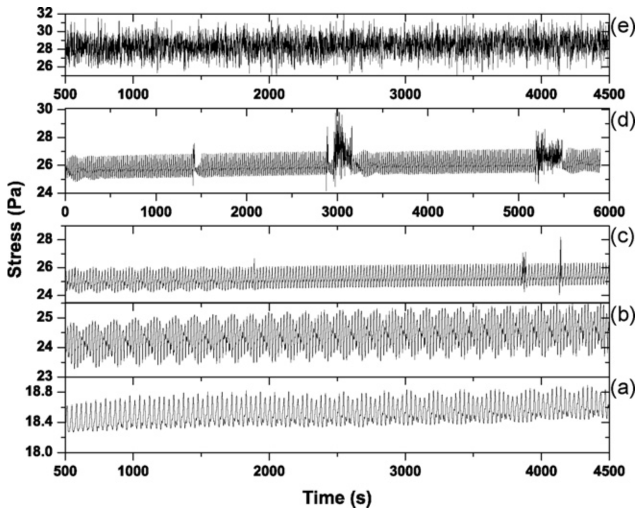

Fig. 13. Stress relaxation at various shear rates for CTAT 2 wt.% + 100 mM NaCl during a different run. (a) $\dot{\gamma} = 10\,s^{-1}$, (b) $\dot{\gamma} = 20\,s^{-1}$, (c) $\dot{\gamma} = 21\,s^{-1}$, (d) $\dot{\gamma} = 22\,s^{-1}$, and (e) $\dot{\gamma} = 23\,s^{-1}$.

Here A_1 and A_2 are the initial and final values, x_0 the center and τ_0 is the time constant. The stress overshoot happens on a time scale of the order of the Maxwell time which for the CTAT 2 wt.% + 100 mM NaCl sample is ≈1 s (Fig. 3b) and can be understood in the following manner: for times smaller than the Maxwell time ($\omega > \omega_{co}$, ω_{co} is the crossover frequency) the system behaves more like a elastic solid and the stress increases rapidly with shear rate. For times larger than the Maxwell time the system behave more like a viscous liquid and hence the stress decreases to a steady value. Stress overshoots have been observed in a variety of systems [49–52] and the sigmoidal decay, terminology borrowed from first order phase transitions, after the overshoot is assumed to be due to the 1-dimensional growth and nucleation of the shear-induced phase. Fig. 12b–d shows the stress overshoot and the decay (sigmoidal fit shown by circles) to a steady stress value. At higher shear rates the stress shows an overshoot and decay followed by complex oscillations Figs. 12e–h. We do not observe overshoots in the pure

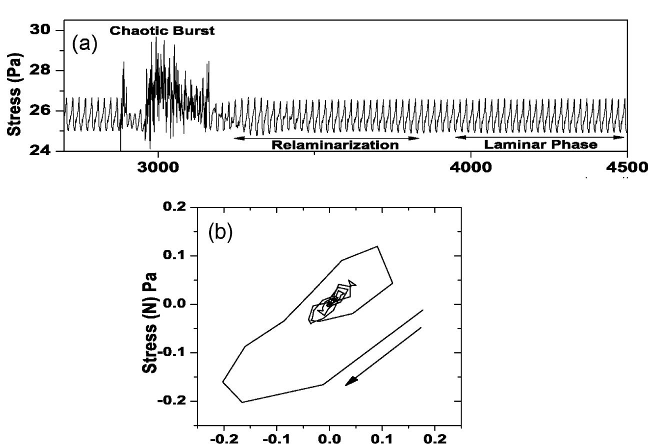

Fig. 14. (a) Expanded stress relaxation dynamics corresponding to data shown in Fig. 13 at $\dot{\gamma} = 22\,s^{-1}$. (b) First return Poincare plot for (a). The arrow shows the spiraling direction. Figure adapted from Ref. [30].

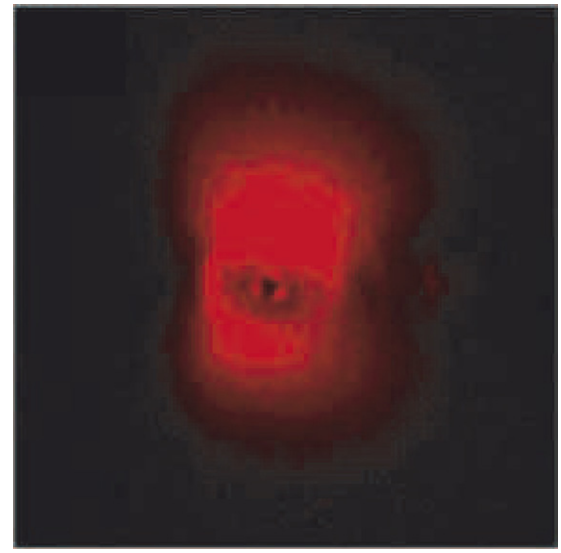

Fig. 15. VH-scattered intensity for the CTAT 2 wt.% + 100 mM NaCl sample.

CTAT 2 wt.% and CTAT 2 wt.% + 10 mM NaCl (this agrees with Bandyopadhyay et al. findings on pure CTAT 2 wt.% [7,31]) both of which happen to be highly non-Maxwellian. All systems CTAT 2 wt.% systems with $c_{NaCl} > 25$ mM showed stress overshoots followed by sigmoidal decay in the initial stress

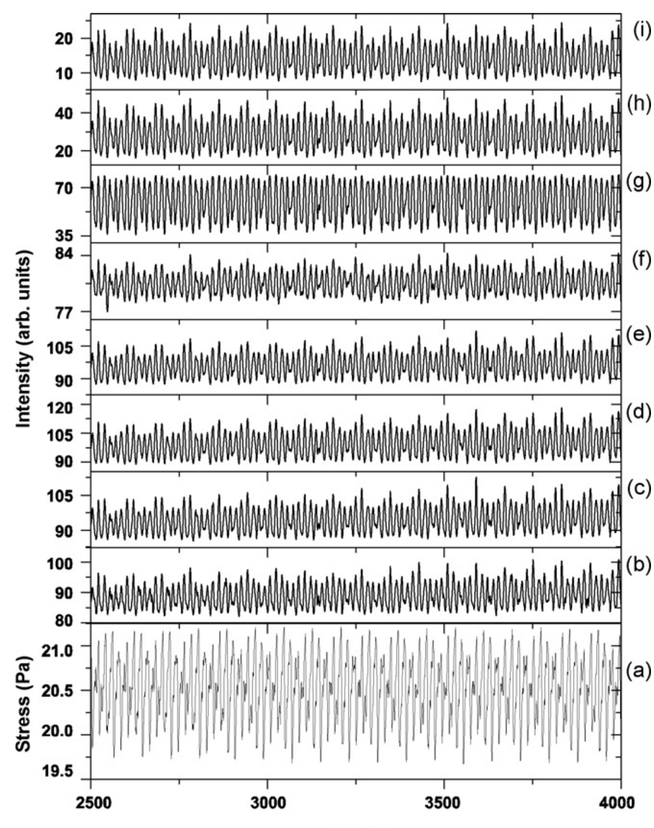

Fig. 16. (a) Stress time series for the CTAT 2 wt.% + 100 mM NaCl sample during a different run. VH intensity at different wave vectors corresponding to the stress time series (a). (b) 0.058 μm^{-1}, (c) 0.115 μm^{-1}, (d) 0.173 μm^{-1}, (e) 0.231 μm^{-1}, (f) 0.404 μm^{-1}, (g) 0.519 μm^{-1}, (h) 0.634 μm^{-1}, and (i) 0.749 μm^{-1}.

response. It is worth mentioning here that for salt concentrations $c_{\mathrm{NaCl}} > 25$ mM, the CTAT + NaCl gels are Maxwellian [31].

Fig. 13 shows the stress relaxation dynamics for the CTAT 2 wt.% + 100 mM NaCl sample. Analogous to the CTAT 2 wt.% + 50 mM NaCl sample, we see quasiperiodicity at $\dot{\gamma} = 20\,\mathrm{s}^{-1}$. At higher shear rates we see intermittent behaviour. Fig. 14a shows the expanded time series of data shown in Fig. 13d at $\dot{\gamma} = 22\,\mathrm{s}^{-1}$. Once again, the nature of the signal during the laminar phase rules out Type-III intermittency, since, for this type of intermittency there is a subharmonic mode with increasing amplitude. We follow the method described in [53] and reconstruct a Poincaré plot by taking the successive minima of the stress in the laminar region after a chaotic burst. In Fig. 14b, we plot the value of the stress at the Nth minimum against its value at the $(N-1)$th minimum. This plot exhibits a spiraling behaviour characteristic of Type-II intermittency. The spiraling behaviour is time-inverted and we call this time-inverted Type-II intermittency after [54] who found similar behaviour in a semiconductor laser with external feed back. The above behaviour implies that the system oscillates back to the laminar phase after a disturbance that caused a burst event.

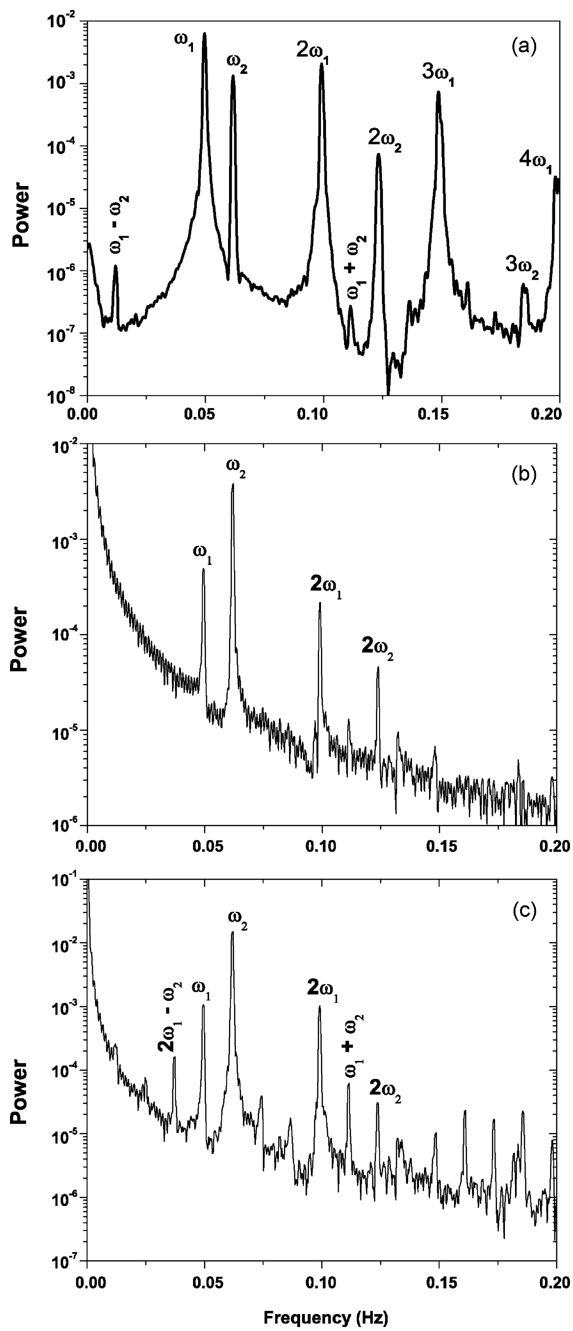

Fig. 17. (a) Fourier power spectrum of the stress time series shown in Fig. 16a. Fourier power spectrum of the VH intensity time series shown in Fig. 16b and c at two wave vectors. (a) $0.173\,\mu\mathrm{m}^{-1}$ and (b) $0.519\,\mu\mathrm{m}^{-1}$.

We will now briefly describe the results of SALS measurements done simultaneously with rheological measurements. The results have been discussed in detail in [30]. The appearance of an *anisotropic* VH scattering pattern in our SALS measurements (Fig. 15) at the onset of shear-thinning implies a high degree of orientational ordering. Fig. 16b–i shows the time series of the VH-scattered intensity at eight different wave vectors for the stress relaxation time series shown in Fig. 16a. At all wave vectors the VH intensity time series follows the stress qualitatively. Fig. 17b and c shows the Fourier power spectrum of the VH intensity time series at two different wave vectors. Both the spectra show the same primary frequencies centered around $\omega_1 = 0.049$ Hz and $\omega_2 = 0.061$ Hz and their higher harmonics. These frequencies are identical to those found in the Fourier spectra of the stress signal (Fig. 17a). Fig. 17a and b also shows other frequency components that are linear combinations of ω_1 and ω_2. These extra features are hallmark of a two-frequency quasiperiodic signal [55].

4. Conclusions

To summarize, our experiments show intermittency in stress relaxation dynamics for systems with coupling between flow and concentration. We have also shown that the normal force and the depolarised scattered (VH) intensity at various wave vectors show dynamics similar to the dynamics seen in stress oscillations. In all our experiments, the "butterfly" pattern is always accompanied by intermittency in stress dynamics. Analysis of the "butterfly" intensity pattern shows that the two bright lobes oriented along the flow direction correspond to a wave vector at which the stress relaxation time is equal to the relaxation time due to concentration fluctuations. This is in excellent agreement with theoretical predictions [41]. We believe it is essential to have flow–concentration coupling to observe the rich dynamics we have seen since, this could provide a mechanism by which mechanical shear banding instabilities could cross over to shear-induced demixing instabilities [13,38]. To the best of our knowledge, there are no theoretical models that predict temporal intermittency in the stress for wormlike micelles that show shear banding. Interestingly, in the rheochaos model by Fielding and Olmsted [13], spatio-temporal intermittent behaviour is seen for moderate to strong coupling strength between the flow and the micellar length. Spatio-temporal intermittency route to chaos has also been predicted by [11]. A complete theoretical understanding for temporal intermittent behaviour in systems that show flow–concentration coupling is lacking at the moment. We hope

Please cite this article in press as: R. Ganapathy, A.K. Sood, Nonlinear flow of wormlike micellar gels: Regular and chaotic time-dependence of stress, normal force and nematic ordering, J. Non-Newtonian Fluid Mech. (2007), doi:10.1016/j.jnnfm.2007.05.008

that our results will motivate further experiments and theoretical modeling.

References

[1] N.A. Spenley, M.E. Cates, T.C.B. McLeish, Phys. Rev. Lett. 71 (1993) 939.
[2] R. Makhloufi, J.P. Decruppe, A. Ait-Ali, R. Cressly, Europhys. Lett. 32 (1995) 253.
[3] R.W. Mair, P.T. Callaghan, Europhys. Lett. 36 (1996) 719.
[4] M.E. Cates, S.J. Candau, J. Phys.: Condens. Matter 2 (1990) 6869.
[5] M.E. Cates, Macromolecules 20 (1987) 2289.
[6] C. Grand, J. Arrault, M.E. Cates, J. Phys. II (France) 7 (1997) 1071.
[7] R. Bandyopadhyay, G. Basappa, A.K. Sood, Phys. Rev. Lett. 84 (2000) 2022.
[8] R. Hegger, H. Kantz, T. Schreiber, The TISEAN Pacakage, may be publicly downloaded from http://www.mpipks-dresden.mpg.de/tisean.
[9] P. Grassberger, I. Procaccia, Phys. Rev. Lett 50 (1983) 346.
[10] P. Grassberger, I. Procaccia, Physica D 9 (1983) 189.
[11] B. Chakrabarti, M. Das, C. Dasgupta, S. Ramaswamy, A.K. Sood, Phys. Rev. Lett. 92 (2004) 055501.
[12] M. Das, B. Chakrabarti, C. Dasgupta, S. Ramaswamy, A.K. Sood, Phys. Rev. E 71 (2005) 021707.
[13] S.M. Fielding, P.D. Olmsted, Phys. Rev. Lett. 92 (2004) 084502.
[14] D.A. Head, A. Ajdari, M.E. Cates, Phys. Rev. E 64 (2001) 064509.
[15] A. Aradian, M.E. Cates, Europhys. Lett. 70 (2005) 397.
[16] M.E. Cates, D.A. Head, A. Ajdari, Phys. Rev. E 66 (2002) 025202.
[17] R. Bandyopadhyay, A.K. Sood, Europhys. Lett. 56 (2001) 447.
[18] P. Fisher, Rheol. Acta 39 (2000) 234.
[19] A.S. Wunenburger, A. Colin, J. Leng, A. Arneodo, D. Roux, Phys. Rev. Lett. 86 (2001) 1374.
[20] J.-B. Salmon, A. Colin, D. Roux, Phys. Rev. E 66 (2002) 031505.
[21] L. Courbin, P. Panizza, J.-B. Salmon, Phys. Rev. Lett. 92 (2004) 018305.
[22] D. Lootens, H. Van Damme, P. Hébraud, Phys. Rev. Lett. 90 (2003) 178301.
[23] M.R. López-Gonzaleź, W.M. Holmes, P.T. Callaghan, P.J. Photinos, Phys. Rev. Lett. 93 (2004) 268302.
[24] W.M. Holmes, M.R. López-Gonzaleź, P.T. Callaghan, Europhys. Lett. 64 (2003) 274.
[25] J.-B. Salmon, S. Manneville, A. Colin, Phys. Rev. E 68 (2003) 051504.
[26] L. Bécu, S. Manneville, A. Colin, Phys. Rev. Lett. 93 (2004) 018301.
[27] H. Azzouzi, J.P. Decruppe, S. Lerouge, O. Greffier, Eur. Phys. J. E 17 (2005) 507.
[28] S.M. Fielding, P.D. Olmsted, Phys. Rev. Lett. 96 (2006) 104502.
[29] S. Lerouge, M. Argentina, J.P. Decruppe, Phys. Rev. Lett. 96 (2006) 088301.
[30] R. Ganapathy, A.K. Sood, Phys. Rev. Lett. 96 (2006) 108301.
[31] R. Bandyopadhyay, A.K. Sood, Langmuir 19 (2003) 3121.
[32] Y. Pomeau, P. Manneville, Commun. Math. Phys. 74 (1980) 189.
[33] C. Jeffries, J. Perez, Phys. Rev. A 26 (1982) 2117.
[34] M. Dubois, et al., Phys. Rev. Lett. 51 (1983) 1446.
[35] J.-Y. Huang, J.-J. Kim, Phys. Rev. A 36 (1987) 1495.
[36] J.F.A. Soltero, J.E. Puig, Langmuir 11 (1995) 3337.
[37] A.K. Sood, R. Ganapathy, Pramana-J. Phys. 67 (2006) 33.
[38] S.M. Fielding, P.D. Olmsted, Eur. Phys. J. E 11 (2003) 65.
[39] V. Schmitt, C.M. Marques, F. Lequeux, Phys. Rev. E 52 (1995) 4009.
[40] J.F. Berret, D.C. Roux, G. Porte, P. Lindner, Europhys. Lett. 25 (1994) 521.
[41] E. Helfand, G.H. Fredrickson, Phys. Rev. Lett. 62 (1989) 2468.
[42] S.T. Milner, Phys. Rev. Lett. 66 (1991) 1477.
[43] M. Doi, A. Onuki, J. Phys. II (France) 2 (1992) 1631.
[44] I.A. Kadoma, J.W. van Egmond, Phys. Rev. Lett. 76 (1996) 4432.
[45] I.A. Kadoma, J.W. van Egmond, Langmuir 13 (1997) 4551.
[46] M.S. Turner, M.E. Cates, J. Phys.: Condens. Matter 4 (1992) 3719.
[47] H.G. Schuster, Deterministic Chaos, VCH, Weinheim, 1988.
[48] H.S. Greenside, G. Ahlers, P.C. Hohenberg, R.W. Walden, Physica D 5 (1984) 322.
[49] J.-F. Berret, Langmuir 13 (1997) 2227.
[50] J.F.A. Soltero, F. Bautista, J.E. Puig, O. Manero, Langmuir 15 (1999) 1604.
[51] F. Bautista, J.F.A. Soltero, J.H. Pérez-López, J.E. Puig, O. Manero, J. Non-Newton. Fluid Mech. 94 (2004) 57.
[52] S. Lerouge, J.-P. Decruppe, P. Olmsted, Langmuir 20 (2004) 11355.
[53] P. Bergé, Y. Pomeau, B. Vidal, Order Within Chaos, Hermann, Paris, 1984.
[54] J. Sacher, Wolfgang Elsser, E.O. Gbel, Phys. Rev. Lett. 63 (1989) 2224.
[55] E. Ott, Chaos in Dynamical Systems, Cambridge University Press, Cambridge, 1993.

Please cite this article in press as: R. Ganapathy, A.K. Sood, Nonlinear flow of wormlike micellar gels: Regular and chaotic time-dependence of stress, normal force and nematic ordering, J. Non-Newtonian Fluid Mech. (2007), doi:10.1016/j.jnnfm.2007.05.008